PROCEEDINGS, 49th Workshop on Geothermal Reservoir Engineering
Stanford University, Stanford, California, February 12-14, 2024
SGP-TR-227

Unveiling Reservoir Fluid Property Dynamics: An Integrated Time-lapse Seismic Tomography and Microgravity Analysis in the Ulubelu Geothermal Field, Indonesia

Aditya A. Juanda, Sotarduga S. Nainggolan, R.M. Tofan Sastranegara, Mulyanto, and Jayanti Anggraini

PT Pertamina Geothermal Energy Tbk., Grha Pertamina, Pertamax Tower 5th floor, Medan Merdeka Timur 11-13. Jakarta, 10110, Indonesia

adityajuanda@pertamina.com

Keywords: Microearthquake (MEQ), Velocity, Tomography, Microgravity, Geothermal, Reservoir

ABSTRACT

Geophysical monitoring technologies, such as Microearthquake (MEQ) and Microgravity, have been consistently employed to observe fluid dynamics in the Ulubelu geothermal reservoir over the past decade during its exploitation phase. The primary objective of this research is to monitor changes in the reservoir's fluid properties, specifically its velocity and density, resulting from production and injection activities. MEQ monitoring utilized eight surface sensors, while Microgravity measurements were conducted at over 105 local sites encompassing production and injection zones, as well as the broader Ulubelu field. The latest additions of 110 MW power plants from unit 3 and 4 involves the introduction of additional injection fluids to the newly established injection pads in the southern section of the field. To oversee the impact of production and injection activities on the reservoir, continuous Microearthquake (MEQ) and periodic Microgravity monitoring was conducted. Throughout the monitoring duration, MEQ recorded more than 12,800 observations of P and S waves. Earthquakes with gap angles of less than 180 degrees were selected for analysis, and the initial 1D velocity structure's shallow portion was determined using various sonic log readings. Ray tracing calculations were carried out using the pseudo-bending technique, and the tomographic parameters, including grid geometry and damping, were assessed through a checkerboard resolution test, yielding satisfactory outcomes. The microgravity data collected during monitoring exhibited very good quality, with an average precision and repeatability of around 15 microgal. The time-lapse tomography results revealed a distinct high ΔVp/Vs value near the injection pads with geometry trending relatively W – E at the reservoir level (+0.05 relative to initial velocity value). This discovery was consistent with the time-lapse microgravity result, which also identified as strong increase in gravity anomalies (up to 40 microgal). These anomalies were attributed to the introduction of fluids from injection wells, indicating that most of the fluids flowed toward the production zone controlled by proven major geological fault with trend NW-SE, while some portions moved in a southeastward direction. The integration of time-lapse seismic tomography and microgravity analysis stands out as a crucial tool for reservoir management in geothermal fields.

1. INTRODUCTION

Indonesia possesses a noteworthy geothermal potential, with PT Pertamina Geothermal Energy (PGE), Tbk., currently overseeing 13 contract areas throughout the country. Sumatra Island, hosting numerous geothermal fields, stands out due to its abundance of volcanoes along the Great Sumatra Fault (GSF), which has a Northwest–Southeast trend. Past research, as indicated by Sieh & Natawidjaja (2000) and Muraoka et al. (2010), characterizes the GSF as a dextral slip fault type. This fault is interpreted as a highly permeable zone, contributing to the formation of an active volcanic arc along its lineaments (Figure 1). These studies provide valuable insights into fault mechanics, associated volcanic activity, and the potential for extracting geothermal energy.

The Ulubelu field, positioned at the southern tip of Sumatra Island and approximately 125 km away from Bandar Lampung city, is characterized as a water-dominated geothermal field. Presently, the Ulubelu field contributes 220 MW of electricity through four power plant units. The latest additions, unit 3 and 4, each with a capacity of 55 MW, have been operational since 2016 and 2017, respectively (Purwono & Nugroho, 2021). In response to this situation, continuous Microearthquake (MEQ) and periodic Microgravity monitoring was conducted to investigate how velocity and mass changes within the reservoir evolve over time.

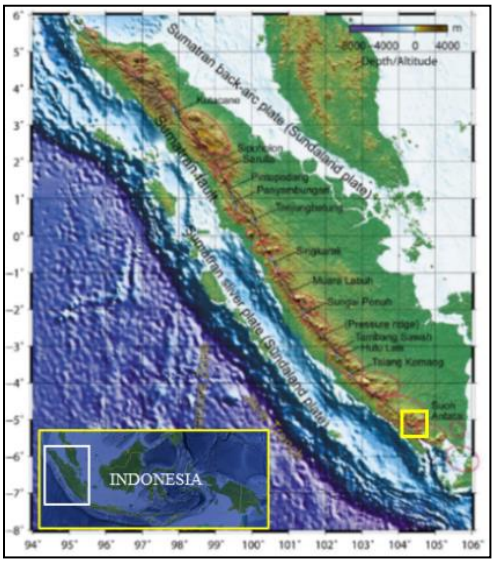

Figure 1 Regional view of the volcanic arc along the Great Sumatran fault (Muraoka, et al., 2010). The Ulubelu field location is indicated by the yellow rectangle shape.

2 GEOPHYSICS MONITORING OVERVIEW

Since 2017, the MEQ network, comprising eight surface geophones, has been implemented to monitor seismic activities around the Ulubelu field. Each geophone is equipped with three components and possesses a natural frequency of 4.5 Hz. The data is recorded using a 24-bit SMART-24® series digitizer with a sampling rate of 200 samples per second (sps). Notably, the production and injection pads in Ulubelu are strategically positioned, with the production pads located in the northern part and the injection pads in the southern part (Figure 2). It is noteworthy that injection activities, specifically in pad R1 and R2 in the southernmost area, commenced in 2017. The spatial coverage of the MEQ network encompasses all production and injection pads, with a sensor spacing of approximately 4 - 5 km.

In line with the MEQ monitoring, microgravity monitoring was conducted in both 2017 and 2018 to assess the gravity variations within the reservoir. Utilizing 105 permanent benchmarks with spatial distance around 500 meters (Figure 2), the relative gravity changes were measured using the Scintrex CG-5 instrument. In addition, groundwater monitoring involved nine shallow wells that drilled up to 60 m depth.

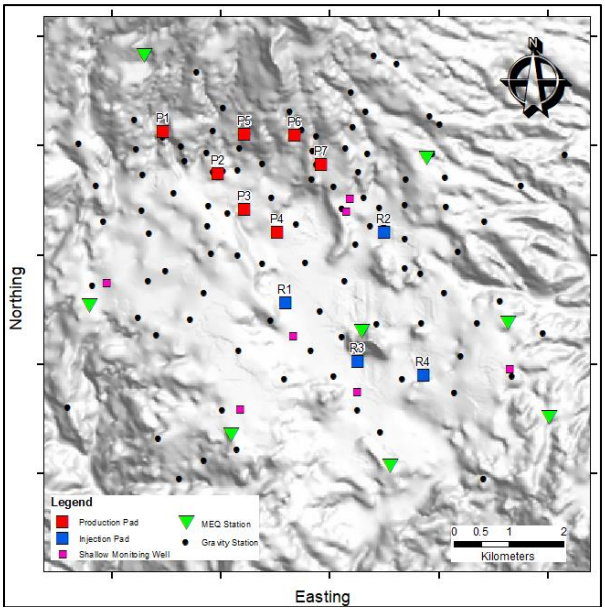

Figure 2 Geophysics Monitoring Network in Ulubelu Field. The MEQ and Gravity Stations cover all the Production and Injection pad with some Shallow Monitoring wells.

3. MICROEARTHQUAKE (MEQ) MONITORING

3.1. Data Acquistion, Phase Observations and Picking Routine

A total of 12,882 observations of P&S waves were recorded during the epochs of 2017 and 2018. Notably, the observations in 2018 constitute 70% of the total, with the remaining 30% attributed to the year 2017. The substantial increase in observations during the 2018 epoch can be attributed to the increased volumes of injection fluids resulting from the additional power generation activities carried out by units 3 and 4. The identification of P and S wave arrival times was accomplished through an automated picking routine utilizing the SAPS seismological data acquisition and processing system (Oncescu et al., 1996). Subsequently, manual phase picking was employed to validate the obtained results. It is noteworthy that the average spatial error for all MEQ events averages less than 0.35 kilometers.

3.2 Earthquake Distribution

As depicted in Figure 3, the majority of MEQ events are concentrated in the proximity of injection wells (R1, R3 and R4), along with several production wells aligning with the primary feed zone elevation (-0.5 to -1 km). The lower MEQ intensity observed in the 2017 epoch is attributed to the initial stages of injection activities at pad R3 and R4, coinciding with an additional power generation capacity of 110 MW. In contrast, during the 2018 epoch, a substantial increase in MEQ intensity is evident in the vicinity of injection pads, particularly at R3 and R4. Notably, the intensity at pads R1 and R2 remains within the same range as the 2017 epoch. However, a distinct MEQ pattern is observed, trending in the NW-SE direction towards production pads (P3 and P4). This pattern signifies the reactivation of the subsurface fault or fracture system within the reservoir, primarily induced by stress perturbations resulting from the introduction of injection fluids near production pads, coupled with fluid withdrawal from producing wells.

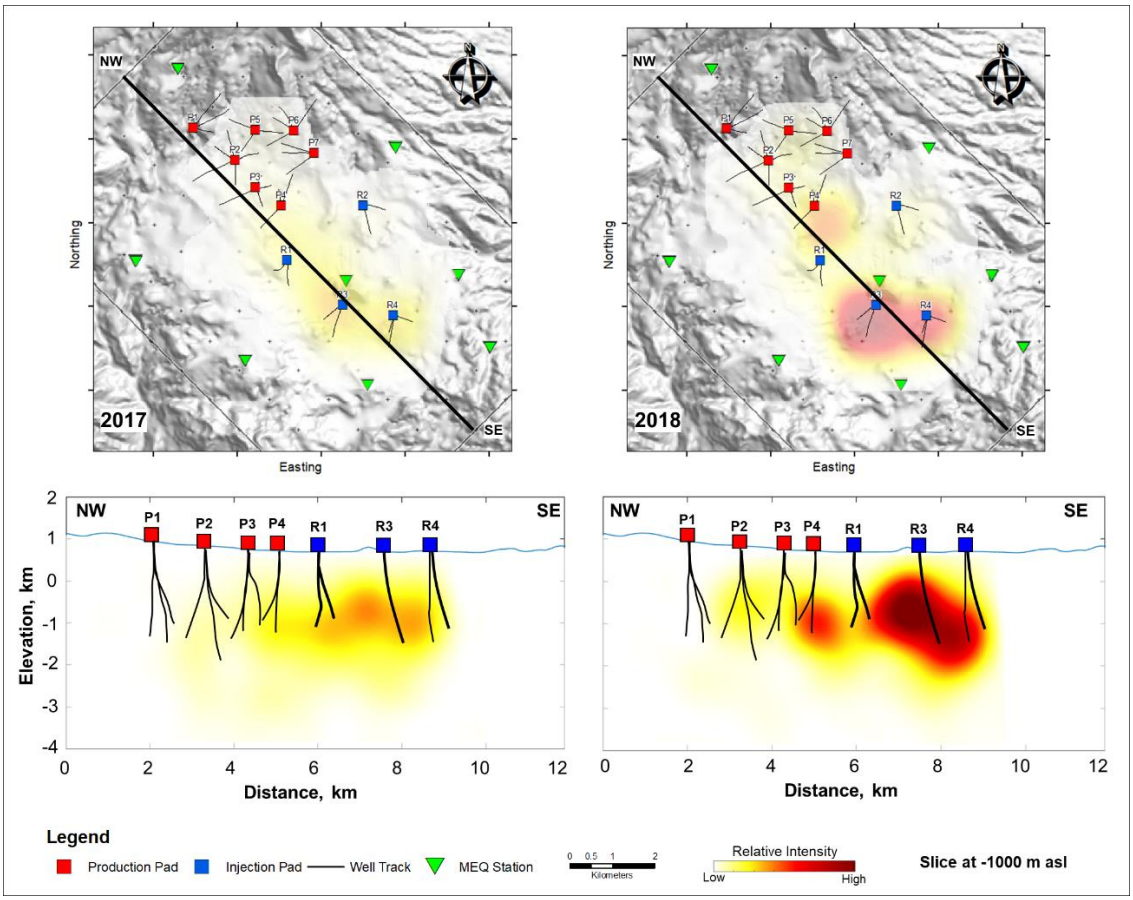

Figure 3 MEQ Events Intensity Map from Epoch 2017 and 2018. Darker shades on the color scale indicate higher intensity, majority of MEQ events are concentrated in the vicinity of injection pads, at feed zone level.

3.2 Velocity Model

The 1-D layered velocity structure for P-wave and S-wave employed in this investigation is divided into two segments, as illustrated in Figure 4 (left). The construction of the shallower segment of the 1-D layered velocity structure relies on sonic log data and lithology distribution obtained from well drilling information. On the other hand, the deeper segment is deduced from the widely accepted earth velocity model, namely the Preliminary Reference Earth Model (PREM) (Dziewonski and Anderson, 1981). Notably, the Vp/Vs ratio utilized in this study is determined as 1.71 through the analysis of the Wadati diagram, as depicted in Figure 4 (right).

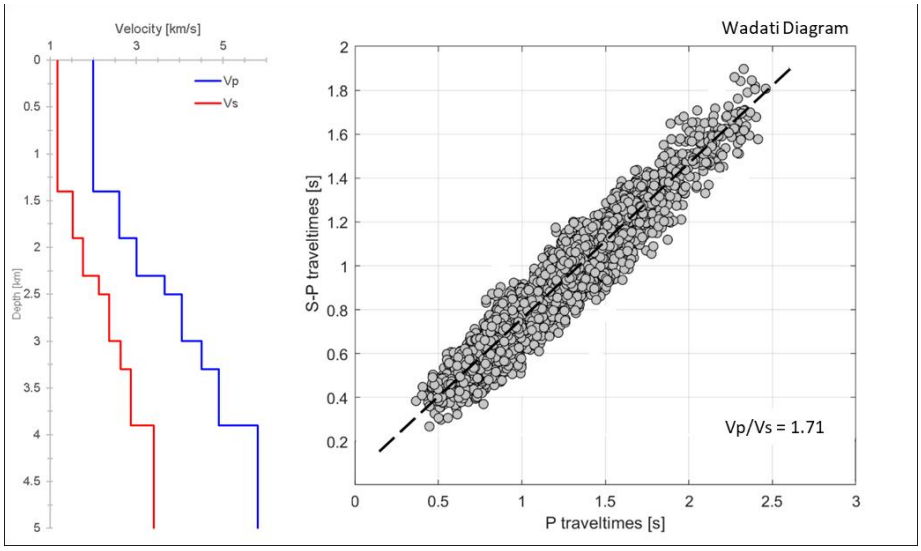

Figure 4 Wadati Diagram (left) and 1-D layered velocity structure (right). The Vp/Vs ratio used is 1.71.

3.4. Seismic Tomography

The proposed approach for examining spatial and temporal velocity variations due to production and injection activities involves the application of seismic tomography. Previous research (Gritto et al., 2013), demonstrated a successful application of seismic tomography in constructing velocity structures. Similarly, other applications successfully employed this technique to accurately delineate the velocity changes within geothermal reservoirs (Gunasekera et al., 2003). In this current study, the SIMULPS12 program (Evans et al., 1994) was utilized for the tomographic inversion, complemented by PGE's proprietary software for data and model preparations, as well as result visualization.

The general framework for the three-dimensional seismic tomography inversion in this study is depicted in Figure 5. The workflow encompasses three primary segments: Data Preparation, Model Grid Parametrizations, and Model Recovery Test and Inverse Modeling. Each of these stages adheres to a consistent set of parameters, ensuring the preservation of model integrity across epoch datasets for subsequent time-lapse seismic tomography analyses.

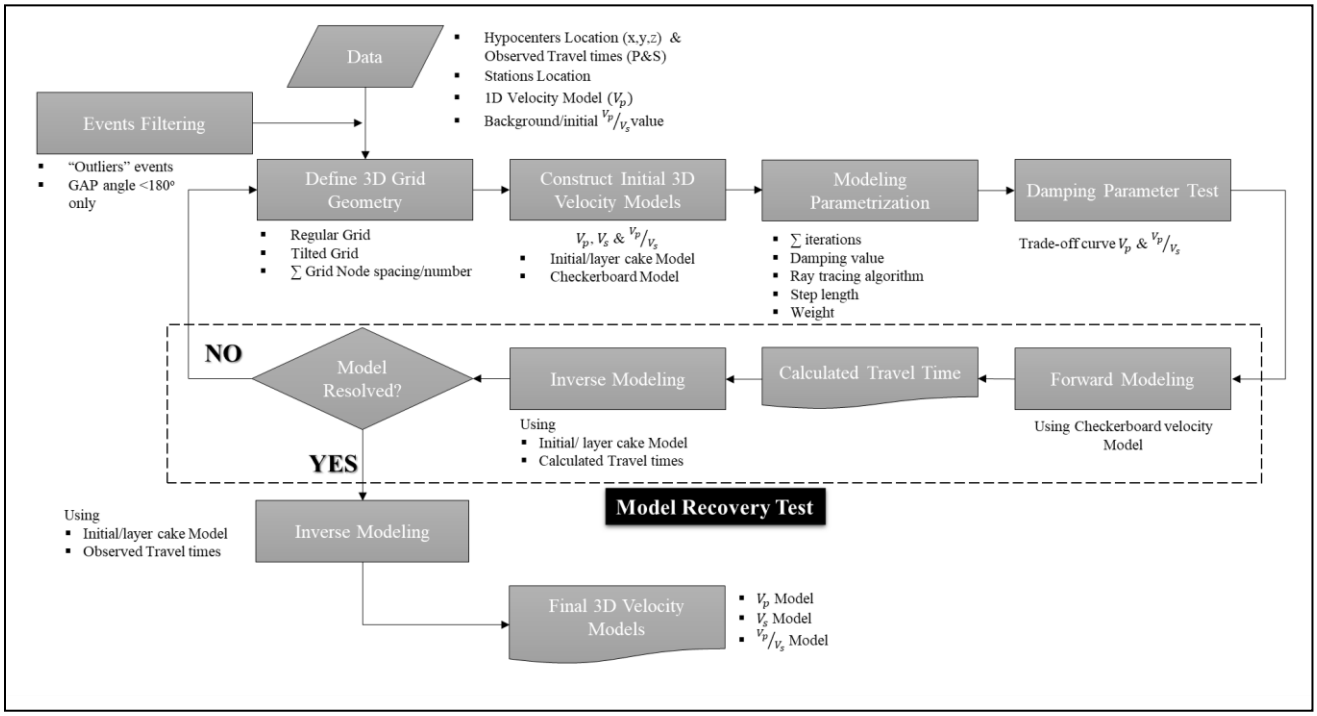

Figure 3 Generalized Three-dimensional Seismic Tomography Inversion Workflow.

3.4.1 The Data Preparation

The initial phase involves the preparation of input data, encompassing hypocenter location, observed travel times for P and S waves, station locations, a 1D velocity model of Vp, initial Vp/Vs values, and events filtering. All MEQ data utilized in this study adheres to an azimuthal gap angle less than 180 degrees or located within the network coverage, thereby minimizing uncertainties in the tomographic model.

3.4.2 The Model Grid Parametrizations

The subsequent stage focuses on defining 3D grid geometry, constructing initial 3D velocity models, modeling parametrizations, and conducting damping parameter tests. The chosen ray tracing algorithm for the inversion process is the Pseudo-bending Approximate Ray Tracing (Um & Thurber, 1987). To accommodate the distribution of MEQs within the Ulubelu area, the grid undergoes a rotation with an azimuth of N 45° W (Figure 6). The grid node spacing is maintained at a regular 1-kilometer interval for the core area, while the background area exhibits a gradual spacing increase up to 50 kilometers, totaling 1650 grid nodes for each Vp and Vp/Vs model. An integral aspect of the tomography inversion process involves determining appropriate damping values through the analysis of damping trade-off curves (Figure 7). The selection of optimal damping values is achieved empirically, considering a broad range of damping values and plotting data misfit versus model variance (Eberhart-Phillips, 1986), with a focus on attaining the best compromise between reducing data misfit and minimizing model variance (Braeuer et al., 2012).

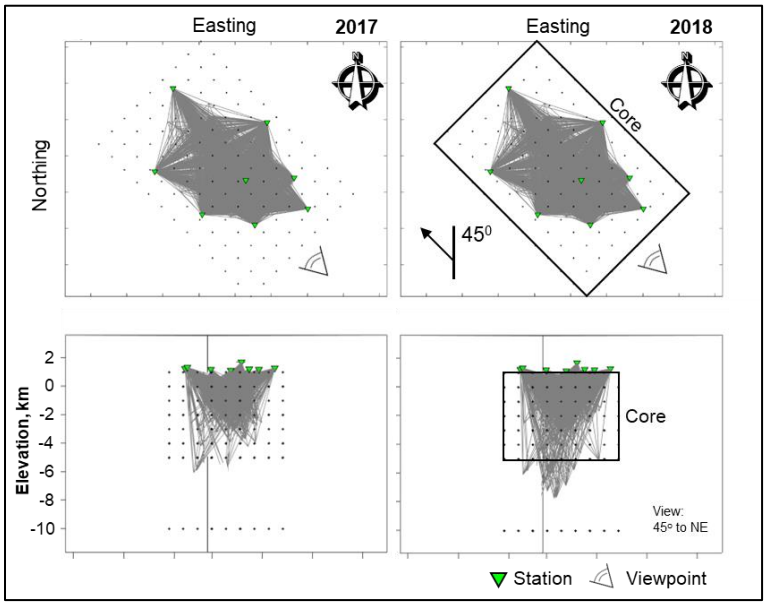

Figure 4 Grid configuration used in tomographic inversion. The grid azimuth is N 45º W.

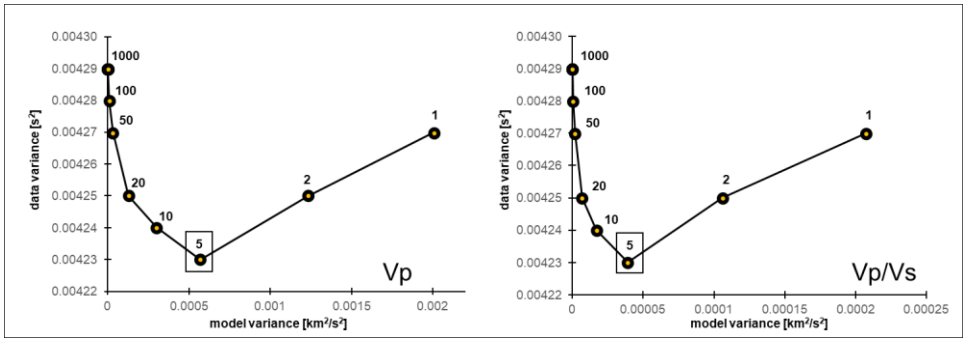

Figure 5 Damping Trade-off Curves. The optimum damping values for Vp and Vp/Vs model is 5.

3.4.3 The Model Recovery Test

The model recovery test is designed to evaluate the ability of the parameters used during tomographic inversion to resolve structural details and identify areas of good resolution (Figure 8). This test was done by preparing a synthetic checkerboard model with ±10% perturbation from the initial velocity model, followed by the calculation of P and S wave travel times using this model (forward modeling). The inversion process employs the calculated travel times and the initial velocity model (layer cake model). Delineation of the good resolution area involves comparing the recovered model to the objective model (checkerboard model), with inverted cells or grid nodes

successfully recovering the objective model values considered as part of the good resolution area. The outcome of this test suggests that the regions characterized by good resolution are consistent across the different epochs. Based on the result, it is inferred that the time-lapse seismic tomography can be analyzed further.

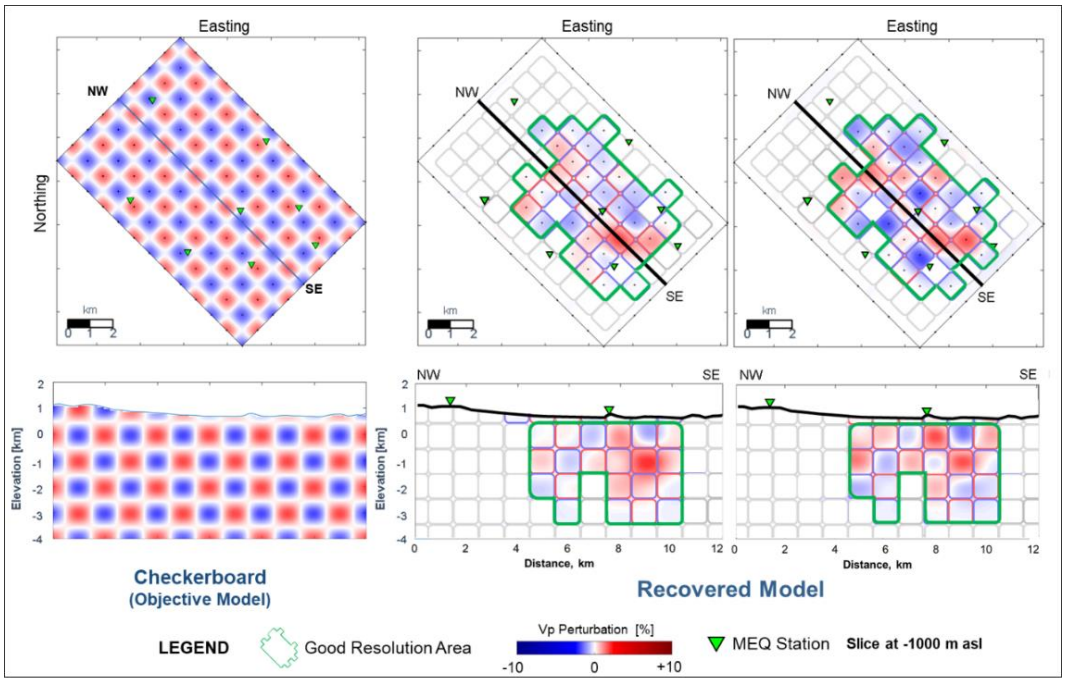

Figure 8 Model recovery test result from epoch 2017 and 2018 epoch. Note that the regions characterized by good resolution are consistent across the different epochs.

4 MICROGRAVITY MONITORING

4.1 Data Acquisition

The closed polygon technique was employed for gravity station measurements, ensuring the reliability and repeatability of the data for all 105 permanent benchmarks. Each station underwent a minimum of two measurements during the survey, and if the repeatability exceeded 0.010 mGal, additional measurements were conducted until satisfactory results were obtained. Throughout the survey, linear drift adjustments were applied based on the assumption of a linear drift between each repeat measurement of the base station. To mitigate non-linear drift, each closed loop was measured within a 4-hour timeframe. Following the correction for tidal effects using Longman's method (1959), the processed data revealed an average drift of 15 microgal per loop.

An additional factor contributing to the observed anomalies in gravity is the influence of groundwater changes. Allis and Hunt (1986) note that changes in gravity linked to fluctuations in groundwater levels can range from tens to hundreds of microgals. To monitor these effects in the field, nine shallow monitoring wells with a depth of 60 meters were employed. Concurrently, the Trimble R-8 GPS Geodetic instrument was utilized to track surface deformation induced by production and injection activities. The static differential method, incorporating multiple fixed benchmarks located outside the reservoir area, was employed to detect potential changes in the local benchmarks at Ulubelu. To attain high-precision GPS data, each dGPS baseline underwent a measurement period of at least 4 hours to ensure substantial satellite data collection. However, for benchmarks positioned under a canopy, a leveling survey was conducted on those specific stations. The combined dGPS and leveling surveys yielded elevation data with an accuracy of 2.1 cm.

4.2 Gravity Data Processing

The Scintrex CG5 utilized in this field is a relative gravity meter, measuring gravity changes in relation to a local reference station, as it does not provide absolute gravity measurements. Given that the reference station is positioned within the reservoir zone near the production pad, it is susceptible to the effects of mass extraction. To mitigate this, three background stations situated outside the Ulubelu field, presumed to be unaffected by geothermal exploitation, were employed to monitor any variations in the local reference station. The regional gravity measurements were utilized to calculate a gravity adjustment that needs to be applied to all local benchmarks. In this particular instance, an adjustment of 13 microgals was added to the previously recorded data.

Notably, the high precision dGPS data depicted minimal changes, as shown in Figure 9. The average elevation change registered a mere 1 cm, with the maximum observed change reaching 4 cm. While approximately 20 stations observed elevation changes ranging from 3 cm to 4 cm, this variance falls marginally beyond the accuracy limit of the dGPS, prompting the decision not to implement elevation correction to the gravity data.

Gravity measurements were consistently conducted during the months of June and July, characterized by relatively low precipitation. Consequently, the monitoring wells primarily captured minor fluctuations in water level depth, as depicted in Figure 10. In alignment with the approach taken for elevation correction, adjustments for shallow meteoric water were also withheld from the gravity data.

Taking into consideration the drift observed in gravity measurements, minor subsidence in certain areas of the field, and the potential impact of shallow groundwater, the estimated detection limit for the microgravity data is approximately 10 microgals. Consequently, the microgravity survey is unlikely to reveal any changes below its detection limit. However, should disparities surpass the detection limit significantly, further attention should be paid to interpreting the reservoir hydrology.

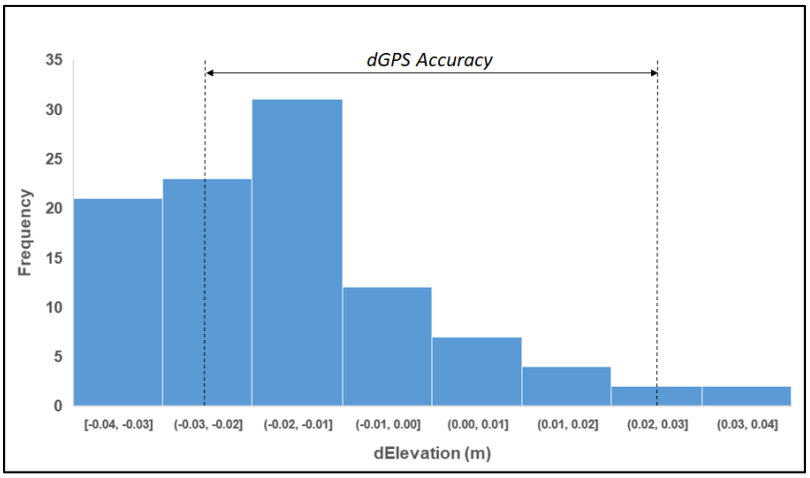

Figure 9. The distribution of elevation changes of 105 permanent benchmarks in Ulubelu

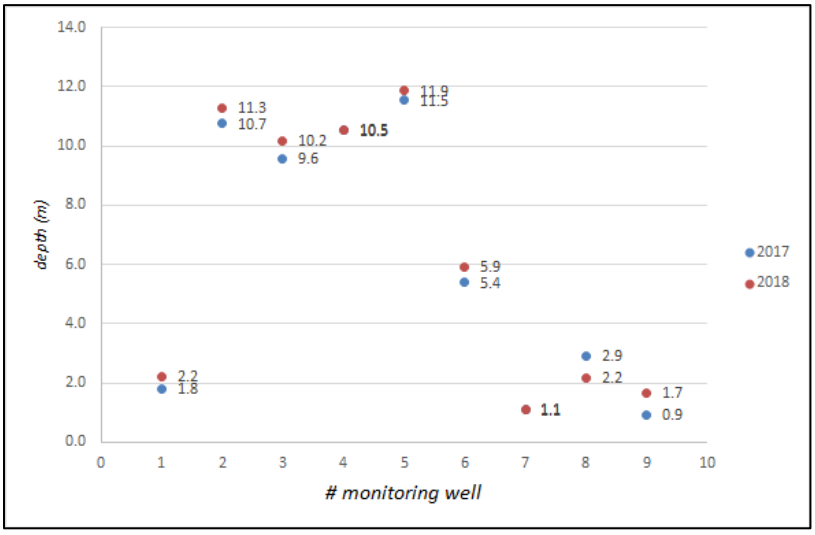

Figure 10. Ground water level from the nine shallow monitoring wells in Ulubelu.

5. RESULT AND DISCUSSION

Production and injection activities are closely linked to changes of the local stress field and mass changes caused by fluid substitution processes, directly associated with the fluid composition in the reservoir rocks. To accurately depict the spatial and temporal dynamics of this phenomenon, the analysis of the Vp/Vs ratio from MEQ data proves to be an effective effort. Notably, Moos and Zoback (1983) observed an increase in the Vp/Vs ratio in fractures saturated with fluids. Conversely, Gunasekera et al. (2003) found that the replacement of pore liquid with vapor (steam) in geothermal reservoirs leads to a reduction in the Vp/Vs ratio. These findings align with the conclusions drawn by Boitnott and Kirkpatrick (1997), suggesting that a high Vp/Vs ratio signifies a wet/water phase reservoir, whereas a low Vp/Vs ratio indicates a dry/steam phase reservoir. From gravity perspective, generally, a positive anomaly indicates a net mass gain in the reservoir due to the injection water, marginal recharge, or cold water downflow. Conversely, the presence of a negative anomaly signifies a net loss of mass, attributed to either fluid extraction or phase changes resulting from the boiling of water to steam within the reservoir. (Allis and Hunt, 1986).

5.1 Time-lapse Seismic Tomography 2017 and 2018 Epoch

This investigation observed consistent tomographic results, particularly in regions exhibiting good resolution, as depicted in Figure 10. During the 2017 epoch, a high Vp/Vs ratio observed was limited to near the R1 injection pad. This phenomenon coincided with the actual injection activities from Unit 1 and 2 primarily into pads R1 and R2. Simultaneously, the beginning of injection activities at pads R3 and R4 did not lead to a significant change in the Vp/Vs ratio. In the subsequent 2018 epoch, a notable change in the distribution of Vp/Vs ratios occurred. Two zones exhibit a notable increase in the Vp/Vs ratio. The first zone is situated near pads R3 and R4, while the second zone encompasses pads R1 and R2, extending into the production area proximate to pads P4, P7, P6, and P5. In contrast, negligible changes in the Vp/Vs ratio are observed in the vicinity of production pads P3, P2, and P1.

To enhance the Vp/Vs ratio changes, a time-lapse tomography analysis has been employed. This involves subtracting each model corresponding to a specific epoch (2018 to 2017). The warm colors, indicative of negative anomalies, signify reservoir conditions characterized by high temperature and steam saturation. Conversely, the cool colors, representing positive anomalies, signify reservoir conditions featuring low temperature and water or liquid saturation. As depicted in Figure 11, the Time-lapse model reveals a distinct and extensive positive ΔVp/Vs anomaly (+0.05 relative to initial velocity value) represented by cool colors, trending from West to East in the southern direction of injection pads R1, R3, and R4, particularly at the major feed zone level (elevation -1 kilometer). These anomalies distinctly indicate the presence of a reservoir saturated with cold water from injection activities. Additionally, a strong negative ΔVp/Vs anomalies (-0.05 relative to initial velocity value) are observed at elevation -2 kilometers beneath production pads, especially in the proximity of pads P1 and P2. This signals the existence of a high-temperature and relatively steam-saturated reservoir, despite the anomaly being slightly outside the area of good resolution.

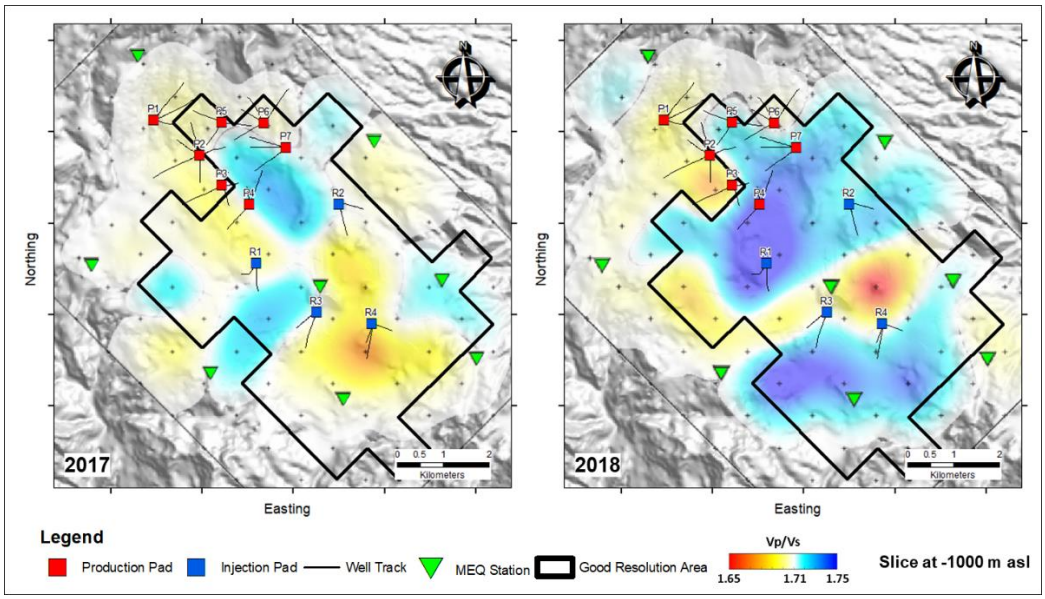

Figure 10 Comparison of Vp/Vs model of epoch 2017 and 2018 at reservoir level (elevation –1 km).

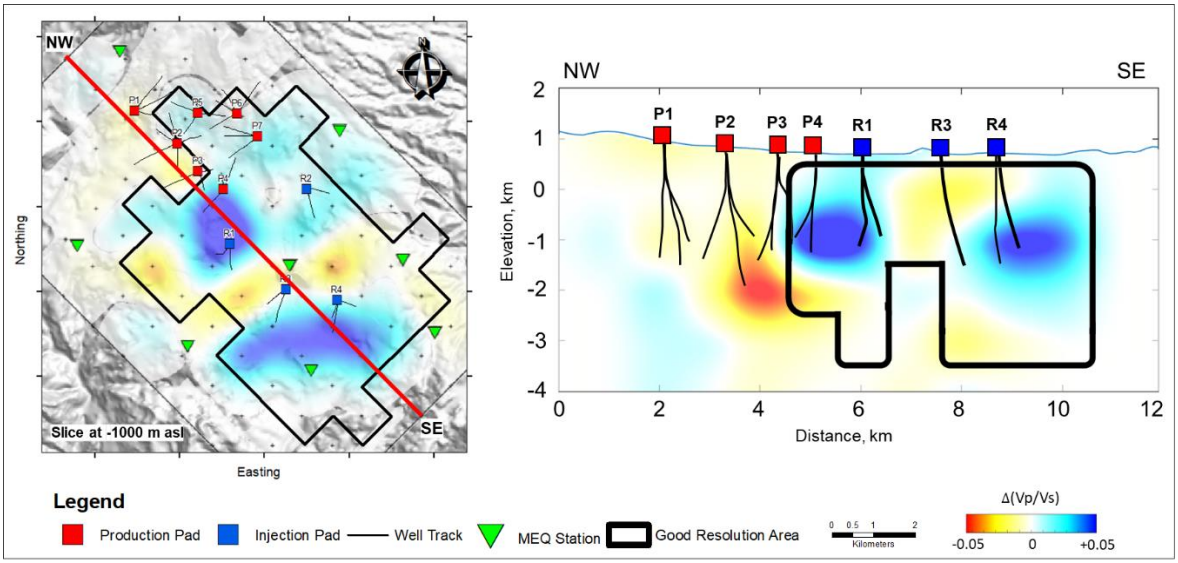

Figure 6 Time-lapse ΔVp/Vs model from Epoch 2018-2017. Black polygon indicates the good resolution area.

5.2 Time-lapse Microgravity

The microgravity anomaly map (Figure 12) was generated through the subtraction of gravity data from each epoch (2018-2017). The cool colors, representing negative anomalies, indicate mass extraction and pressure decrease due to production activities. Conversely, the warm colors, representing positive anomalies, indicate mass addition and pressure increase due to injection.

Over the monitoring period, the anomaly spans from -30 microgal to +40 microgal across the surveyed area. Positive anomalies ranging from 20 to 40 microgal are identified in the vicinity of the injection pads, particularly pads R3 and R4. Additionally, minor injection activities in pad R1 and R2 wells correlate with positive gravity anomalies of up to 20 microgal. This gravity anomaly increase coincides with the significant increase of injection rate in pads R3 and R4, as additional 2x55 MW plants commenced in 2017. The localized positive anomalies in the injection area may also suggest a lack of marginal peripheral recharge during the monitoring period. Conversely, the production zone consistently exhibits negative gravity changes, with measured data indicating a gravity decrease of up to -30 microgal, particularly in pad P2.

This result implies that the area with the most significant mass extraction and pressure decrease, which leads to boiling likely occurred in the vicinity of pads P2, P3, P4, and P7. In certain areas where geothermal fluid is extracted, no observable gravity changes may be attributed to the injected fluid or marginal water directly displacing the extracted mass in the reservoir. However, these subtle anomalies fall below the microgravity data detection limit, necessitating further geochemical and reservoir analyses to explore these potential scenarios.

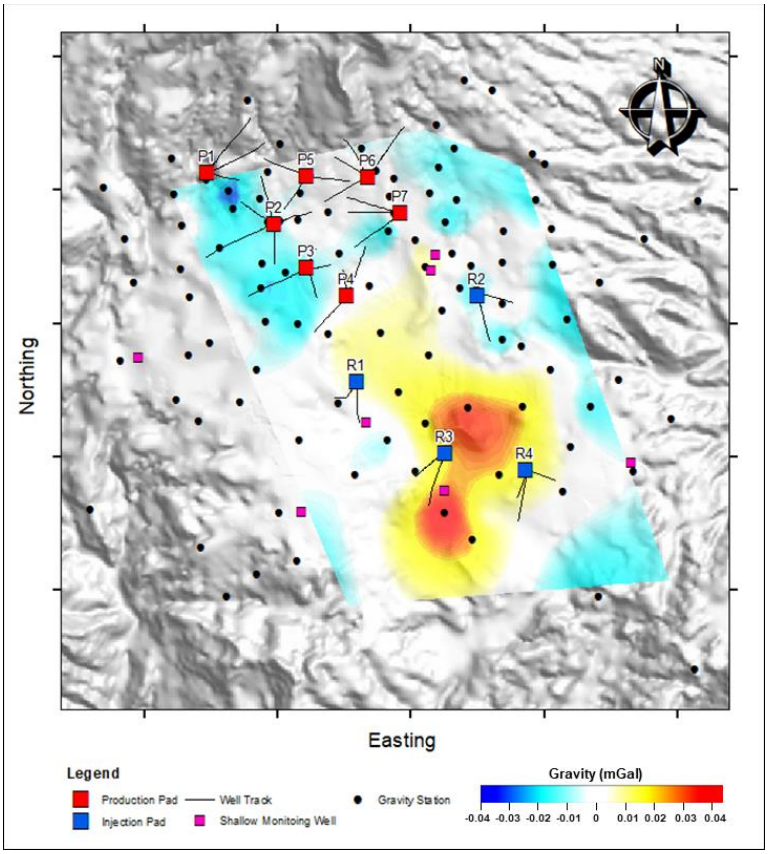

Figure 12 Time-lapse Microgravity map from Epoch 2018-2017.

6. SUMMARY AND CONCLUSIONS

This research showcases the effective utilization of time-lapse seismic tomography and microgravity analysis in characterizing fluid content within a water-dominated geothermal reservoir in the Ulubelu field. The findings highlighting on how the introduction of additional injection fluids results a distinct and widespread high or positive ΔVp/Vs anomalies (+0.05 relative to initial velocity value) and strong positive gravity anomaly (+40 microgal) during the 2018-2017 epoch. This phenomenon is marked by the accumulation of injection water in the vicinity of injection pads, flowing towards the S-SW & SE direction from R3 & R4, and towards the North direction from R1. Furthermore, the results obtained from microgravity analysis consistently align with the findings from time-lapse seismic analysis, both in the proximity of production and injection activities over the monitoring period. Nevertheless, these outcomes necessitate further examination, including comprehensive analyses involving geochemistry, tracer test, and borehole data. In conclusion, the integration of time-lapse seismic tomography and microgravity analysis stands out as a crucial tool for reservoir management in geothermal fields, as underscored by the valuable insights derived from this research.

ACKNOWLEDGEMENT

The study presented here was fully supported by Pertamina Geothermal Energy, Tbk. for providing the data, reviewed the manuscript and granted permission to publish this study.

REFERENCES

Allis, G., Hunt, M., 1986. Analysis of Exploitation-induced Gravity Changes at Wairakei Geothermal Field, Geophysics, Vol. 51, n. 8, 1647-1660.

Boitnott, G. N. & Kirkpatrick, A., 1997. Interpretation of field seismic tomography at The Geysers geothermal field, California. Stanford, Twenty-second Workshop on Geothermal Reservoir Engineering.

Braeuer, B. et al., 2012. High-resolution local earthquake tomography of the southern. *Geophysical Journal International,* Volume 191, p. 881–897.

Dziewonski, A. M. & Anderson, D. L., 1981. Preliminary reference Earth model. *Physics of the Earth and Planetary Interiors,* pp. 25(4), 297–356.

Eberhart-Phillips, D., 1986. Three-dimensional velocity structure in northern California Coast Ranges from inversion of local earthquake arrival times. *Bulletin of the Seismological Society of America.*

Evans, J. R., Eberhart-Phillips, D. & Thurber, C. H., 1994. User's manual for SIMULPS12 for imaging Vp and Vp/Vs: A derivative of the Thurber tomographic inversion SIMUL3 for local earthquakes and explosions, s.l.: U.S. Geological Survey.

Gritto, R., Yoo, S.-H. & Jarpe, S. P., 2013. Three-dimensional Seismic Tomography at the Geysers Geothermal Field, CA, USA. Stanford, Thirty-Eight Workshop on Geothermal Reservoir Engineering.

Gunasekera, R., Foulger, G. R. & Julian, B. R., 2003. Reservoir depletion at The Geysers geothermal area, California, shown by four-dimensional seismic tomography. *Journal of Geophysical Research.*

Longman, I.M., 1959, Formulas for computing tidal accelerations due to the moon and sun. Journal Geophysical Research, 2351-2355.

Moos, D. & Zoback, M. D., 1983. In situ studies of velocity in fractured crystalline rocks. *Journal of Geophysical Research,* Volume 88, p. 2345– 2358.

Muraoka, H. et al., 2010. Geothermal Systems Constrained by the Sumatran Fault and Its Pull-Apart Basins in Sumatra, Western Indonesia. Bali, s.n.

Oncescu, M. C., Rizescu, M. & Bonjer, K. P., 1996. An Automated and Networked Seismological Acquisition and Processing System. *Comput Geosci,* pp. 22 (1), 89–97.

Purwono, N. & Nugroho, A. J., 2021. The Development of Ulubelu Geothermal Power Plant 2x55 MW - Lampung Indonesia. Reykjavik, s.n.

Sieh, K. & Natawidjaja, D., 2000. Neotectonics of The Sumatran Fault, Indonesia. *Journal of Geophysical Research Vol. 10,* pp. 28,295 - 28,326.

Um, J. & Thurber, C., 1987. A fast algorithm for two-point seismic ray tracing. *Bulletin of the Seismological Society of America,* Volume 77, p. 972–986.